ACS Sustainable Chemistry & Engineering

pubs.acs.org/journal/ascecg

Research Article

Ion Transport and Electrochemical Properties of Fluorine-Free Lithium-Ion Battery Electrolytes Derived from Biomass

Inayat Ali Khan,* Oleg Ivanovich Gnezdilov, Andrei Filippov, and Faiz Ullah Shah*

Cite This: *ACS Sustainable Chem. Eng.* 2021, 9, 7769–7780

Read Online

ACCESS | Metrics & More | Article Recommendations | Supporting Information

ABSTRACT: Unlike conventional electrolytes, ionic liquid (IL)-based electrolytes offer higher thermal stability, acceptable ionic conductivity, and a higher electrochemical stability window (ESW), which are indispensable for the proper functioning of Li-ion batteries. In this study, fluorine-free electrolytes are prepared by mixing the lithium furan-2-carboxylate [Li(FuA)] salt with the tetra(*n*-butyl)-phosphonium furan-2-carboxylate [(P_{4444})(FuA)] IL in different molar ratios. The anion of these electrolytes is produced from biomass and agricultural waste on a large scale and, therefore, this study is a step ahead toward the development of renewable electrolytes for batteries. The electrolytes are found to have T_{onset} higher than 568 K and acceptable ionic conductivities in a wide temperature range. The pulsed field gradient nuclear magnetic resonance (PFG-NMR) analysis has confirmed that the $(FuA)^-$ anion diffuses faster than the $(P_{4444})^+$ cation in the neat (P_{4444})(FuA) IL; however, the anion diffusion becomes slower than cation diffusion by doping Li salt. The Li^+ ion interacts strongly with the carboxylate functionality in the $(FuA)^-$ anion and diffuses slower than other ions over the whole studied temperature range. The interaction of the Li^+ ion with the carboxylate group is also confirmed by ^{7}Li NMR and Fourier transform infrared (FTIR) spectroscopy. The transference number of the Li^+ ion is increased with increasing Li salt concentration. Linear sweep voltammetry (LSV) suggests lithium underpotential deposition and bulk reduction at temperatures above 313 K.

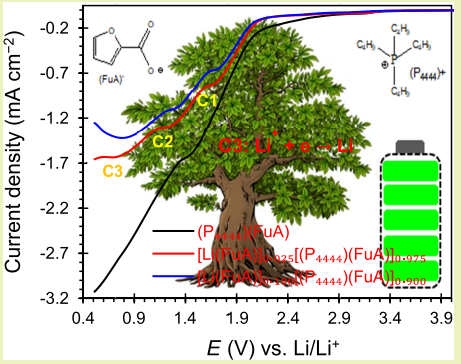

KEYWORDS: *renewable electrolytes, furan-2-carboxylate, ionic conductivity, nuclear magnetic resonance, underpotential deposition*

INTRODUCTION

The lithium-ion battery (LIB) marketplace is emerging at the fastest rate as batteries are identified as high-performance energy storage devices that can efficiently store and deliver energy on demand along with decreasing the carbon footprint of the transportation sector.[1] The portable consumer electronic market is already dominated by LIBs, which have been recognized as the most encouraging energy storage devices for hybrid and fully electric vehicles and for modern mobile energy storage systems.[2] The commercial LIB electrolytes comprise $LiPF_6$ dissolved in organic-carbonate-based solvents that are volatile and flammable and thus cause serious chemical hazards under harsh conditions.[3] $LiPF_6$ is thermally unstable and decomposes at about 343 K in an organic-solvent-based electrolyte.[4−7] $LiPF_6$ is proven to generate HF due to the self-decomposition ($LiPF_6 \rightarrow LiF + PF_5$) and then water hydrolysis ($PF_5 + H_2O \rightarrow POF_3 + 2HF$).[8,9] HF is toxic and corrosive, can react with the cell components, can leach out transition metals from the positive electrode, and can corrode the current collectors. The heat generation and thermal runaway are serious issues, which not only adversely affect the performance of a battery but are also connected to water and soil pollution and human health at the battery recycling stages.[10] The large fluorine contents and the flammable organic solvents need to be replaced with nonfluorinated and nonflammable organic electrolytes to improve the safety and performance of next-generation batteries.

In this regard, new salts were developed during the past few decades,[11−14] but the majority of them were unstable for thermal and electrochemical applications. Later, the Hückel-type anions were developed in the mid-1990s, which were more stable than $LiPF_6$ in the presence of water and even acted as moisture scavengers for organic aprotic electrolytes.[15] Such anions have a great potential in battery applications, and there are still unexplored mechanisms in the aromatically stable lithium salts, having high thermal stability and being readily soluble in organic solvents or ionic liquids (ILs).

There is an urge to develop safe electrolytes for LIB applications. In this scenario, ILs, which are molten salts at room temperature, are nonflammable, and have high thermal stability, are emerging as promising substitutes for the volatile

Received: February 9, 2021
Revised: May 12, 2021
Published: June 1, 2021

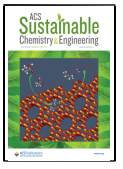

https://doi.org/10.1021/acssuschemeng.1c00939
ACS Sustainable Chem. Eng. 2021, 9, 7769–7780

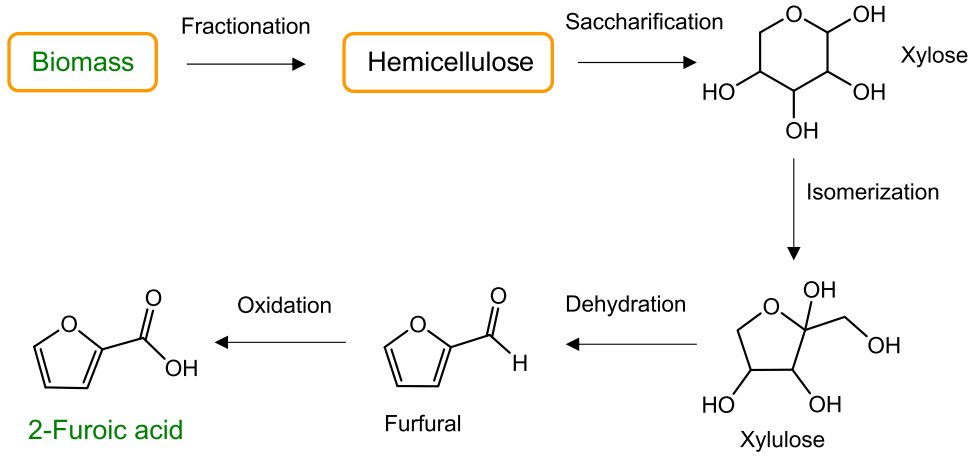

Figure 1. General scheme for the production of 2-furoic acid from lignocellulosic biomass.

organic-solvent-based electrolytes for LIBs. The IL electrolyte adoption may improve the safety and reliability of batteries without affecting their performance.[16] Tetraalkylammonium, cyclic aliphatic quaternary ammonium, and imidazolium were found to be the most effective cations for LIB ILs.[16] Further, small steric hindered ions with asymmetric structures are particularly promising as they show fast ion transportation as well as wide electrochemical stability windows.[16] Among the anions, bis(trifluoromethylsulfonyl)imide (TFSI) and bis-(fluorosulfonyl)imide (FSI) are found to be the most effective for IL-based LIB electrolytes because of their promising physicochemical and electrochemical properties.[16,17]

In our previous study, tetra(*n*-butyl)phosphonium and tetra(*n*-butyl)ammonium coupled with furan-2-carboxylate, tetrahydofuran-2-carboxylate, and thiophene-2-carboxylate anions as emerging new classes of fluorine-free ILs were reported.[18] The effects of aromaticity in furan-2-carboxylate and thiophene-2-carboxylate rings on the thermal and electrochemical stability and ionic mobility are thoroughly investigated using both experimental and theoretical studies.[18] We found that the aromatic furan-2-carboxylate and thiophene-2-carboxylate anions-based ILs with a common cation are thermally and electrochemically more stable than the nonaromatic anion-based IL. Besides green transportation, the development of renewable and environmentally friendly fuel sources is also needed.[19] The biomass conversion into useful chemicals has become an emerging research field during the last decade.[20] The hydrolysis of lignocellulosic biomass leads to monosaccharides such as glucose, fructose, and xylose. The subsequent dehydration of xylose generates 2-furfural,[21] which can be further converted into 2-furoic acid via catalytic oxidation (Figure 1)[22] and into furan via palladium-catalyzed decarbonylation.[23] Furoic acid has been used as a preservative and an acceptable flavoring ingredient in industries for decades.

Encouraged by the sustainability and electrochemical stability, we synthesized and dissolved lithium 2-furoate salt in tetra(*n*-butyl)phosphonium furoate IL in different molar ratios to get electrolytes of varying lithium contents. It is critically important to thoroughly understand the physico-chemical properties of new electrolytes before utilizing them in battery applications. Therefore, systematic thermal stability, ion diffusivity, cation−anion interactions, and thermo-electrochemical stability of all of these electrolytes are investigated in this study.

EXPERIMENTAL SECTION

Synthesis and Electrolyte Preparation. The synthesis and characterization details of the $(P_{4444})(FuA)$ IL are given in our previous publications,[18,24] while the synthesis and characterization details such as nuclear magnetic resonance (NMR) measurements (^{1}H, ^{13}C, ^{31}P, ^{7}Li) and Fourier transform infrared (FTIR) spectra of the lithium salt and the electrolytes are given in the Supporting Information. Li(FuA) salt was mixed with the $(P_{4444})(FuA)$ IL in the concentration range of 2.5−10 mol % to prepare the electrolytes (Table 1). We found 10 mol % of Li(FuA) salt in this IL to be a saturated solution. All samples were dried in a vacuum oven at 333 K for up to 5 days, and the water content was found to be <280 ppm, which was measured by Karl Fischer titration.

Table 1. Composition and Concentration of the Electrolytes Studied

electrolytes	IL (mol %)	salt (mol %)	molality (mol kg^{-1})
$[Li(FuA)]_{0.025}[(P_{4444})(FuA)]_{0.975}$	97.5	2.5	0.070
$[Li(FuA)]_{0.050}[(P_{4444})(FuA)]_{0.950}$	95.0	5.0	0.144
$[Li(FuA)]_{0.075}[(P_{4444})(FuA)]_{0.925}$	92.5	7.5	0.217
$[Li(FuA)]_{0.100}[(P_{4444})(FuA)]_{0.900}$	90.0	10.0	0.305

Nuclear Magnetic Resonance Spectroscopic Analysis. A Bruker Ascend Aeon WB 400 (Bruker BioSpin AG, Fällanden, Switzerland) nuclear magnetic resonance (NMR) spectrometer was used for the structural characterization of the Li salt and the electrolytes. The solution NMR measurements of Li(FuA) salt were performed in deuterated dimethyl sulfoxide (DMSO) using a 5 mm NMR tube. NMR spectroscopy of the electrolytes containing Li(FuA) in $(P_{4444})(FuA)$ IL was carried out by placing the sample in a 5 mm NMR tube, which was then placed in a 10 mm NMR tube containing $CDCl_3$ as an external lock. The working frequency for ^{1}H was 400.21 MHz, for ^{13}C was 100.64 MHz, for ^{31}P was 162.01 MHz, and for ^{7}Li was 155.53 MHz. The ^{7}Li NMR spectra were indirectly referenced to a LiCl aqueous solution of 1 mol L^{-1}. The NMR spectra were processed using the Topspin 3.5 software.

NMR Diffusion and Relaxation Measurements. Pulsed gradient spin echo-nuclear magnetic resonance (PGSE-NMR) experiments were carried out using a Bruker Avance III (Bruker BioSpin AG) NMR spectrometer. ^{1}H and ^{7}Li were used for self-diffusion experiments using a Bruker PGSE-NMR probe Diff50. The diffusional decays (DDs) were measured using the stimulated echo (StE) pulse train. The form of DD for single-component diffusion can be described as[25]

https://doi.org/10.1021/acssuschemeng.1c00939
ACS Sustainable Chem. Eng. 2021, 9, 7769−7780

$$A(\tau, \tau_1, g, \delta) \propto \exp\left(-\frac{2\tau}{T_2} - \frac{\tau_1}{T_1}\right)\exp(-\gamma^2\delta^2 g^2 D t_d) \quad (1)$$

where A is the integral intensity of the signal, τ is the time interval between the first radiofrequency pulse and the second radiofrequency pulse, and τ_1 is the time interval between the second radiofrequency pulse and the third radiofrequency pulse. γ is the gyromagnetic ratio of the magnetic nuclei (^{1}H and ^{7}Li), g is the amplitude and δ is the duration of the gradient pulse, $t_d = (\Delta - \delta/3)$ represents the diffusion time, Δ is the time interval difference between the two identical gradient pulses, and D is the diffusion coefficient of ions. T_1 and T_2 are longitudinal and transverse relaxation times, respectively. The 90° pulse duration was 7 μs, the range of δ was from 0.5 to 2 ms, τ was in the range from 3 to 5 ms, and g was varied from 0.06 up to the maximum possible gradient amplitude, 29.73 T m^{-1}. Diffusion time t_d was changed from 4 to 100 ms for the diffusion of ^{1}H and in the range of 200−700 ms for the diffusion of ^{7}Li. The repetition time during the accumulation of signal transients was 3.5 s.

FTIR Spectroscopic Analysis. The attenuated total reflection Fourier transform infrared (ATR-FTIR) spectra of samples were recorded using a Bruker IFS 80v spectrometer equipped with a deuterated triglycine sulfate (DTGS) detector and diamond ATR accessory. The spectra were recorded by employing the double-side forward−backward acquisition mode. The total number of scans was 256, co-added and signal-averaged at an optical resolution of 4 cm^{-1}.

Thermal Analysis. A PerkinElmer 8000 TGA instrument was used for the thermogravimetric analysis (TGA) using 2−4 mg of each sample in the temperature range of 303−873 K at 10 K min^{-1} under nitrogen as an inert atmosphere. The Pyris software was used to calculate the onset of decomposition temperature, T_{onset}, by taking the intersection of the baseline representing the weight loss and the tangent of the weight vs temperature curve.[26,27]

Electrochemical Characterization. Ionic conductivity and electrochemical stability window (ESW) measurements were carried out using a Metrohm Autolab (PGSTAT302N) electrochemical workstation equipped with an impedance FRA32M module. The TSC 70 closed cell (RHD Instruments, Germany) was used for analyzing about 70 μL of each sample. A temperature-controlled Microcell HC cell stand was used to perform variable-temperature experiments. The cell was polished with a Kemet diamond paste (0.25 μm) before each experiment.

Two-electrode cell assembly, consisting of a glassy carbon working electrode and a Pt cup counter electrode (K_{cell} = 1.486 cm^{-1}), was used for ionic conductivity measurements. Heating and cooling impedances (from 0.1 Hz to 1 MHz) were recorded from 253 to 373 K. Each experiment at a given temperature was started with a 10 min gap of thermal equilibration.

For cyclic voltammetry (CV) and linear sweep voltammetry (LSV), a three-electrode cell assembly consisting of a glassy carbon working electrode (2 mm), a counter electrode (Pt crucible), and a Ag wire pseudoreference electrode (coated with AgCl) was used. CVs were measured at 100 mV s^{-1} and at room temperature, while LSVs were measured at 20 mV s^{-1} and at different temperatures from 293 to 353 K. The potential values were recorded in reference to ferrocene and then shifted to Li/Li$^+$ potential values using $E_{Li/Li^+} = E_{Fc/Fc^+} + 3.2$ V equation.[28] The anodic and cathodic limits from LSVs were defined at a current density of 0.1 mA cm^{-2}.[29]

RESULTS AND DISCUSSION

The lithium furoate salt, Li(FuA), was prepared in a high yield and mixed with tetra(*n*-butyl)phosphonium furan-2-carboxylate ((P$_{4444}$)(FuA)) IL at different concentrations (mol %). The ion structures constituting the corresponding IL and electrolytes and their abbreviations are shown in Figure 2.

Thermal Properties. The thermal stability of the Li salt and the electrolytes was determined using thermogravimetric analysis (TGA), and the corresponding curves are shown in Figure 3a. The first descent in the curves represents the weight loss of up to 79% corresponding to the decomposition of the $(P_{4444})^+$ cation in the IL and in the electrolytes, while the second descent represents the decomposition of the $(FuA)^-$ anion. The values of T_{onset} (from the intersection of the baseline corresponding to the first descent point) are 569, 570, 571, and 571 K for the electrolytes with 2.5, 5, 7.5, and 10 mol % Li(FuA) salt, respectively. The T_{onset} of the neat Li(FuA) salt is at 670 K, almost 100 K higher stability than the electrolytes and also the neat IL (564 K). The thermal stability of the neat (P$_{4444}$)(FuA) IL is comparable to that of EMIFSI and EMITFSI ILs that decompose at around 498 and 648 K, respectively.[30] Both the commercial Li salts, lithium bis(fluorosulfonyl)imide (LiFSI) (>473 K)[31] and lithium bis(trifluoromethanesulfonyl)imide (LiTFSI) (653 K),[32] also have comparable thermal stabilities with Li(FuA). The much higher decomposition temperature of the Li salt can be ascribed to the rigid aromatically stabilized structure of the furan ring that can promote the salt stability. The weight derivatives vs temperature of the IL and the electrolytes are shown in Figure 3b. The neat IL and all of these electrolytes have two inflection points, where the first inflection indicates the point of the greatest rate of change on the weight loss curves. The maximum rate of the weight loss of the neat IL and the electrolytes occurs in the temperature range of 588−593 K, which is associated with the degradation of cations. The addition of Li salt slightly delays the rate of degradation from 588 K for the neat IL to 593 K for the electrolyte with 10 mol % Li salt. The Li salt revealed the highest rate of degradation at about 698 K, showing the highest thermal stability.

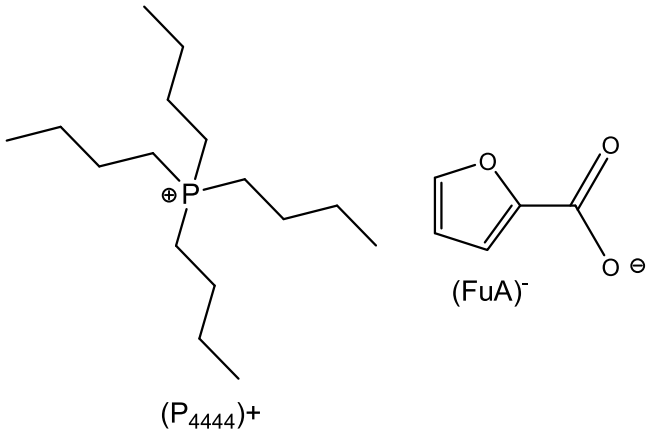

Figure 2. Chemical structures and abbreviations of the IL and the electrolyte components used in this study.

Ionic Conductivity. Figure 4a shows that the temperature-dependent ionic conductivities of the neat IL and the electrolytes are best fitted to the Vogel−Fulcher−Tammann (VFT) model in the entire studied temperature range. The fitted factors abstracted from the VFT equation are given in Table S1. As can be seen in Table S1, the E_σ values are slightly decreasing with an increase in Li salt concentration such as 12.0 kJ mol^{-1} for the 2 mol % electrolyte to 10.2 kJ mol^{-1} for the 10 mol % electrolyte. This is probably due to the contribution of hydrophobic interactions between the neighboring phosphonium ions, which decreased with increasing Li salt concentration. The data shown in Figure 4a indicate that the conductivity of the neat IL is somewhat higher than that of the electrolytes throughout the studied temperature range. Figure 4b shows that the ionic conductivity of the electrolytes decreases as a function of Li salt

https://doi.org/10.1021/acssuschemeng.1c00939
ACS Sustainable Chem. Eng. 2021, 9, 7769−7780

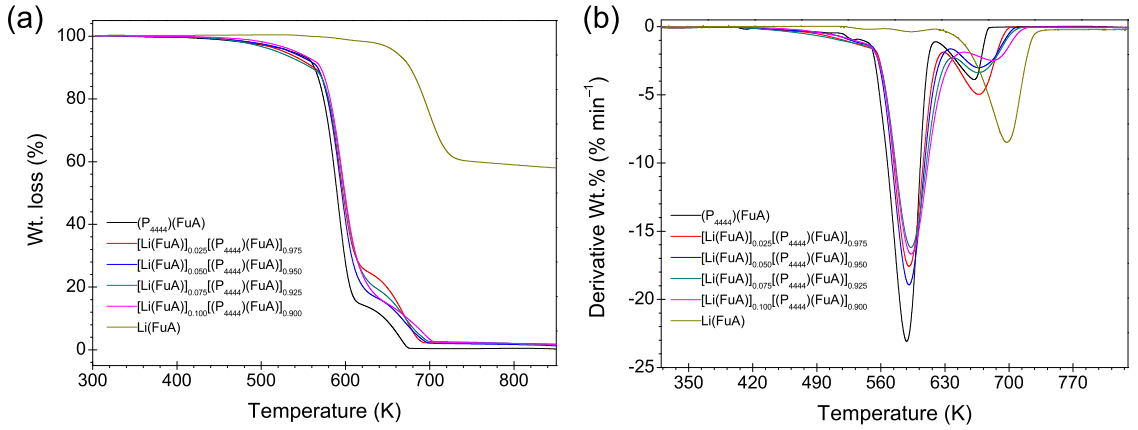

Figure 3. (a) TGA curves and (b) weight loss derivative as a function of temperature for the neat IL, $[Li(FuA)]_x[(P_{4444})(FuA)]_{1-x}$ electrolytes and Li-salt.

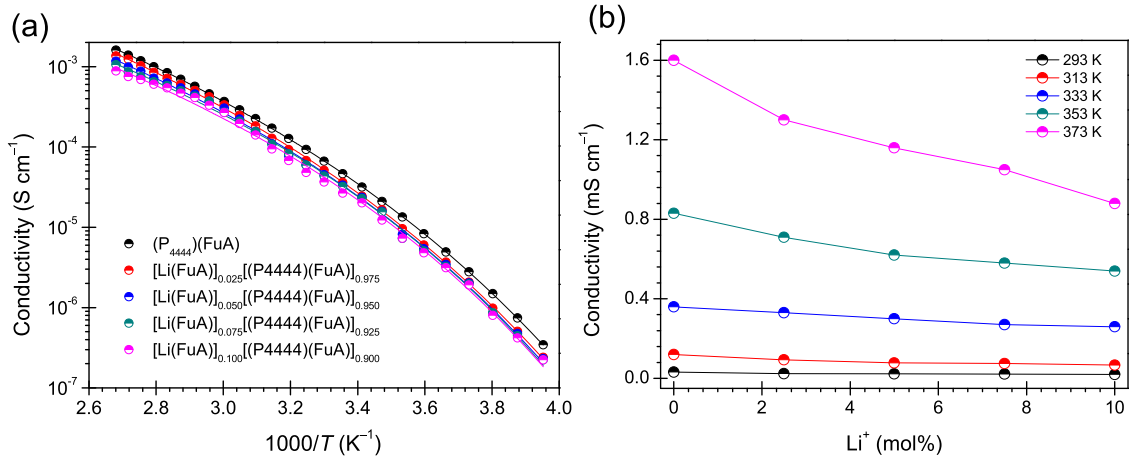

Figure 4. (a) Ionic conductivity vs temperature and (b) ionic conductivity vs the Li^+ concentration of the electrolytes.

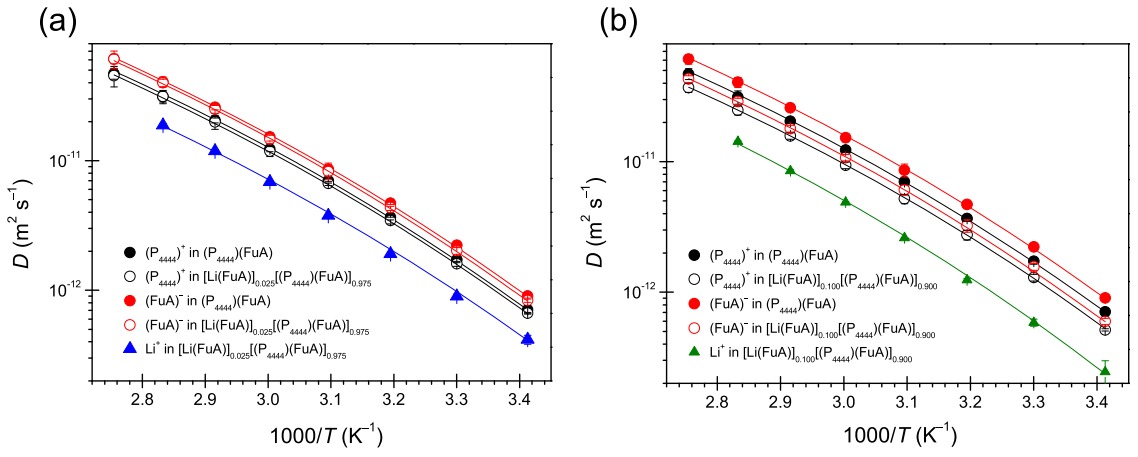

Figure 5. Diffusivity of ions as a function of temperature (a) in the neat IL and in the 2.5 mol % Li electrolyte and (b) in the neat IL and in the 10 mol % Li electrolyte. Experimental data are indicated by symbols, and their best VFT equation fittings are presented by lines.

concentration. This might be due to the decrease in free volume and an increase in the Coulombic interaction between the Li^+ ion and the $(FuA)^-$ anion upon the addition of Li-salt (Figure 4b). A similar effect of Li^+ concentration on the ionic conductivity of electrolytes is observed when Li(MEEA) salt[33] and $Na(NTf_2)$ salt[34] were added to their respective ILs.

NMR Diffusometry. The diffusional decays (*DDs*) of these electrolytes demonstrated a single exponential form (eq 1) over the whole temperature range, which is independent of the diffusion time t_d. Diffusion coefficients are obtained from the experimental *DDs* by fitting to eq 1. The diffusion coefficients of ions for the different Li salt concentrations are different as can be seen in Figures 5 and S8−S10. In a series of previously published reports,[35−44] diffusion of a number of ILs was studied together with some other macroscopic transport properties such as viscosity and ionic conductivity. In these

https://doi.org/10.1021/acssuschemeng.1c00939
ACS Sustainable Chem. Eng. 2021, 9, 7769−7780

studies, a unique diffusion coefficient for each ion has been obtained. Different diffusivities of anions and cations are typical for different protic[45] and aprotic[33,46−52] ILs. The diffusivities of cations and anions were comparable in some of the ILs,[39,48] while in others, cations[36,37,53] or anions[33] diffused faster. It was shown that the molecular size of ions does not directly affect their ionic diffusion coefficients.[36] In the case of the 1-alkyl-3-methylimidazolium bis-(trifluoromethanesulfonyl)imide ILs, higher *Ds* correspond to the cation, even though the effective hydrodynamic radius of the cation is larger than that of the anion.[37] Similarly, the diffusivity of a bulky cation is larger than that of a smaller anion in [EMIm][$EtSO_4$] IL.[53] Such an irregular relationship between the ion sizes and diffusivity was ascribed to the presence of local microstructures in ILs, which results in a cooperative character and finally retards the ion diffusion.

In the studies of $[Li(FuA)]_x[(P_{4444})(FuA)]_{1-x}$ electrolytes, the diffusion coefficients of ions follow the decreasing order of $(FuA)^-$ > $(P_{4444})^+$ > Li^+ (Figures 5 and S8−S10). The sizes (diameters) of ions as calculated from their chemical structures are ∼11.8 Å for $(P_{4444})^+$ and ∼5.2 Å for $(FuA)^-$, while the ionic size of Li^+ is 1.52 Å. Therefore, the ratio of sizes between $(P_{4444})^+$ and $(FuA)^-$ is ∼2.27. Another way to estimate the ratio of sizes of the cation to anion is to consider their molecular masses and to use a spherical approximation of the ion shape. The ratio of molecular masses is 259.43/111.08 ∼2.34, and the ratio of ionic radii is $(2.34)^{1/3}$ ∼1.33. This estimation is rather rough because the deviation of the real form of the ions is not taken into consideration. Figure 5 shows that there is a quantitative correlation between diffusivities and sizes of the cation and the anion in IL; the larger-size cation diffuses slower than the smaller anion. However, in the case of the Li^+ ion, it is the opposite: the diffusion of Li^+ is slower than that of the organic ions despite its smallest size among the ions. The quantitative diffusivities and sizes of $(P_{4444})^+$ and $(FuA)^-$ can be compared by assuming that the viscosity of the surrounding media is equal for both ions. According to the Stokes−Einstein equation (eq 2), the diffusivity is inversely related to viscosity

$$D = \frac{kT}{6\pi\eta R_H} \tag{2}$$

where k is the Boltzmann constant, η is the viscosity, and R_H is the Stokes radius of the diffusing particle (ion). Indeed, the ratio of diffusivities of the cation and anion is nearly 1.25 and does not demonstrate a dependence on the temperature and concentration of Li(FuA) in the system. Therefore, the measured values of the diffusivity of the cation and anion generally agree with their relative sizes. It is known that ions form complexes containing two or more ions in bulk ionic liquids and only a part of the cations and anions is present in the dissociative state.[40] The correlation between the size of ions and their diffusivities can be explained by the fast exchange of the bound (in $(P_{4444})(FuA)$ or their associates) and free states of the cation $(P_{4444})^+$ and anion $(FuA)^-$. In this case, the lifetime of an ion in the associates is much less than the minimal diffusion time of the experiment (4 ms) and the diffusivity of ions in these electrolytes is provided mainly by the relatively fast motion of the free cation $(P_{4444})^+$ and anion $(FuA)^-$.

The ratio of diffusivities of $(P_{4444})^+$ and Li^+ varies from ∼2.4 to 2.6 at lower temperatures and ∼3.6 to 4.6 at higher temperatures with increasing Li(FuA) salt concentration. This can be explained by the long-time ($t \geq t_d$ ∼700 ms) presence of Li^+ in the ionic associates, which has sizes much larger than sizes of the cation and anion, and the sizes are increasing with an increase in the temperature. Therefore, the sizes of Li^+-containing associates are 2.4−4.6 times larger than the sizes of diffusing associates containing $(P_{4444})^+$ cations (or the free cation). In this context, a pertinent question arises: What are the other species present in the associates with Li^+? Obviously, it is Li(FuA), which dissociates only partly, as in the case of $(P_{4444})(FuA)$. Therefore, the diffusing particles may contain $(P_{4444})(FuA)$, Li^+, $(FuA)^-$, and also $(P_{4444})^+$ interacting with $(FuA)^-$.

However, diffusivities of $(FuA)^-$ and $(P_{4444})^+$, which even are contained in associates with Li^+, are higher than that of Li^+ and do not show any dependence on the diffusion time used in these experiments (4−100 ms). Therefore, the lifetime of $(FuA)^-$ and $(P_{4444})^+$ in the complexes with Li^+ as well as the lifetime of the associated state of Li(FuA) is less than 4 ms. This suggests that the Li^+ ion forms a long-living core of the associate, while other components of the associate are in the conditions of fast exchange (in the NMR PGSE time scale) with the surrounding. The presence of such long-living associates formed in the presence of Li salt that are negatively charged has been previously observed in ionic liquids modified by Li salt using electrophoretic NMR.[54] As discussed earlier, the diffusion coefficients measured by ^1H PGSE-NMR are related mostly with $(P_{4444})^+$ and $(FuA)^-$ ions. Therefore, using the Stokes−Einstein equation (eq 2), we can estimate the sizes of the associates that contain Li^+. If the diffusivity of the Li^+ associate is a factor of ∼2.4−4.6 less than that of $(P_{4444})^+$, the size of the latter is larger by the same factor, that is ∼18.8 × (2.4−4.6) = ∼28−54 Å. On the other hand, if we apply the ratio of masses, $M_{associate} = M_{cation} \times (D_{cation}/D_{associate})^3$ ∼ 3580−25 210. If the associate contains up to six anions coordinated by Li^+,[55] its size will be ∼11 Å and its mass will be nearly 670. Therefore, according to the diffusivity data, the size of the associate is a factor of more than 6 times larger than one solvation shell of the anions coordinated by the central Li^+ ion. This might be possible if the associate contains several Li^+ ions with solvation shells of anions (probably of cations as well) bonded by electrostatic as well as hydrogen-bonding interactions.

Another plausible mechanism that can contribute to the lowering diffusivity of Li^+ in this system is that the Li^+ ion loses its re-orientational mobility due to the strong interactions with the surrounding anions. The hopping process of an ion that leads to translational displacement requires re-orientation of the ion, and the loss of the re-orientational rate may lead to a decrease in the translational diffusion coefficient. Orientational and translational dynamics of molecules with a nonspherical form and electrostatic and hydrogen-bonding interactions is a complex process. For small diatomic molecules, translational diffusion is strongly coupled to their rotational dynamics.[56] For complex liquids with larger molecules, such as glycerol and *n*-propanol, the neutron experiments have indicated that the true molecular diffusive motion is a mixed translational−rotational−vibrational displacement.[57] For (2-hydroxyethyl)-trimethylammonium bis(trifluoromethylsulfonyl)imide IL, the simulated correlation function comprises two independent domains:[35] the short-time performance declines within the picosecond time interval determine re-orientational correlation

https://doi.org/10.1021/acssuschemeng.1c00939
ACS Sustainable Chem. Eng. 2021, 9, 7769−7780

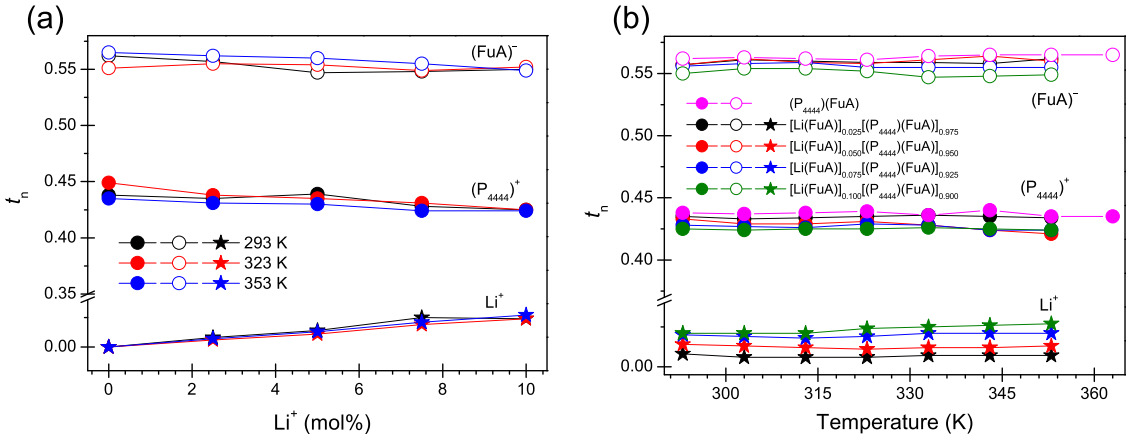

Figure 6. Apparent transfer numbers as a function of (a) Li salt concentration and (b) temperature for the neat (P_{4444})(FuA) IL and the electrolytes.

times, while the long-range nanosecond interval is actually accredited to the translational diffusion.

Coming back to our electrolytes, an increase in Li(FuA) concentration leads to a repetitive decrease in the diffusion coefficients of all ions (Figures 5 and S8−S10). The degree of the decrease in the diffusion coefficients is ∼0.7 over the whole range of Li(FuA) concentration from 2.5 to 10 mol % in the IL. A similar effect was previously observed for different ILs and polymer electrolytes,[33,44,51,52,54,58] which has been explained by the association of ions induced by Li^+ and the formation-extended alkali-anion complexes.[42,44,54,59] Despite the smallest size of Li^+, it diffuses slowly compared to the organic cations and anions, which is in great agreement with the previous studies.[42,44] If it is an effect of ion association between the Li^+ and the $(FuA)^-$ anion, then why the presence of Li^+ does not decrease the diffusivity of the $(FuA)^-$ anion to the same extent as that of Li^+ diffusivity? There are two possibilities: first, the much higher molar fraction of $(FuA)^-$ compared with Li^+ results in the presence of free $(FuA)^-$ anions that can diffuse faster, and second, the exchange between the associated and the free $(FuA)^-$ is fast in the NMR PGSE time scale (<4 ms) and therefore no significant contribution of the associated $(FuA)^-$ anions is observed in the diffusion decays of these ions.

An increase in temperature leads to a monotonous increase in the diffusivity of all ions due to the thermal activation of translational mobility. An Arrhenius-type equation describing temperature-dependent D_s is given as follows

$$D(T) = D_0 \cdot \exp\left(\frac{-E_D}{RT}\right) \tag{3}$$

where D_0 is a temperature-independent parameter, E_D is the diffusion molar activation energy, and R represents the gas constant. Generally, the Arrhenius function shows a linear dependence $D(T)$ in Arrhenius coordinates. However, non-Arrhenius dependences were observed for $(P_{4444})^+$, $(FuA)^-$, and Li^+ ions as can be seen in Figure 5. Such a non-Arrhenius dependence is also reported for many ILs.[33,36−39,44,51,52,59] The reason for this is the proximity of the glass transition temperature of the ionic liquid, T_0, to the temperatures of measurements. In such cases, eq 4, a Vogel−Fulcher−Tammann (VFT)-type equation for diffusion, is usually used[60−62]

$$D = D_0 \exp\left(\frac{-B}{(T - T_0)}\right) \tag{4}$$

where T_0 and B represent adjustable parameters, while the energy of activation for diffusion is related to B as we know that $E_D = B \times R$. This form corresponds to the Arrhenius dependence in the high-temperature limit ($T_0 \to 0$). We have presented $D(T)$ in Figure 5 by fitting D_0, T_0, and B using eq 4. Keeping in mind that the glass transition temperature is a property of a system and not of any distinct ion, we applied this fitting to temperature dependences of Li^+ ions as well, in spite of the fact that its temperature dependences look like Arrhenius dependences (Figures 5 and S10). The solid lines in Figures S8−S10 show the best results of the fitting, and the obtained fitting parameters are shown in Table S2.

The ion transference number is a fraction of the total electrical current carried by a given ionic species in an electrolyte. It depends on the fraction, charge, and translational mobility of a specific ion. Generally, the presence of Li^+ ions in an electrolyte changes the transference numbers of all ions of the system. Equation 5 was used to determine the apparent transference numbers of the individual ions in the neat IL and in the electrolytes.[63,64]

$$t_i = \frac{x_i D_i}{\sum_i x_i D_i} \tag{5}$$

where t_i represents the apparent transference number, x_i is the molar fraction of each ion, and Di represents the self-diffusion coefficient of each ion. It is noteworthy that the transference number determined from NMR analysis is usually called the transport number. This is due to the fact that diffusion coefficients determined from PFG-NMR are an average contribution from both the individual charged species (isolated ions) and the neutral species in the form of aggregates. The aggregates are diffusing slower due to their larger radius than the individual charged ions, thus leading to an inferior diffusion coefficient and smaller transference number of each ion measured. This is also one of the explanations that the transference numbers determined from electrochemical techniques are usually double as large as those determined from PFG-NMR diffusometry.[65]

The values of the t_i of Li^+, $(P_{4444})^+$, and $(FuA)^-$ ions as a function of Li(FuA) concentration and temperature are shown in Figure 6. The t_i of the $(FuA)^-$ anion is larger than that of the

https://doi.org/10.1021/acssuschemeng.1c00939
ACS Sustainable Chem. Eng. 2021, 9, 7769−7780

$(P_{4444})^+$ cation, revealing a faster diffusion of the anion compared with the $(P_{4444})^+$ cation. The transference number of Li^+ is lower due to its lower fraction and lower diffusivity than the organic ions. The transference number of the Li^+ ion is increasing linearly with an increase in Li salt concentration with a mean slope of 0.0027 per mole of the added Li(FuA) salt, while the transference number of the $(P_{4444})^+$ cation decreases with a mean slope of 0.0012 per mole. However, the transference number of the $(FuA)^-$ anions remains unchanged. This is credited to the high Li number density and low fraction of the $(P_{4444})^+$ cation.[66] An increase in the temperature does not reveal any significant change in the transference numbers of ions. This means that the mobilities of ions change in a concerted way, while the microscopic structure of the system and exchange conditions do not change in the studied temperature range.

^{7}Li NMR and Infrared Spectroscopy. The mobility of Li^+ within the neat electrolytes and its interactions with the $(FuA)^-$ anion are investigated through ^{7}Li NMR and FTIR spectroscopy (Figure 7 and Figure 8). In the ^{7}Li NMR spectra,

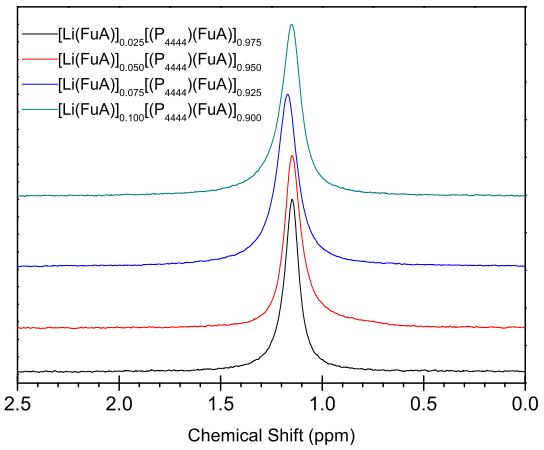

Figure 7. ^{7}Li NMR spectra of the $[Li(FuA)]_x[(P_{4444})(FuA)]_{1-x}$ electrolytes.

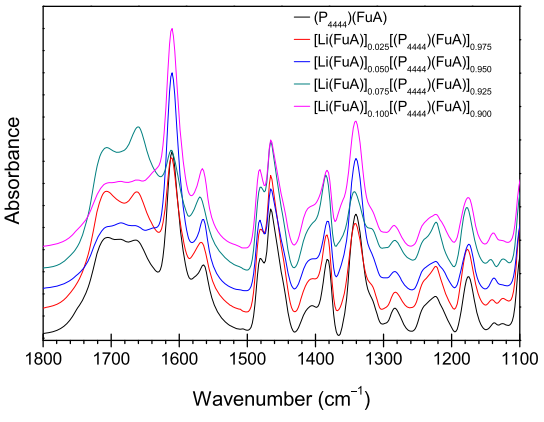

Figure 8. ATR-FTIR spectra of the $[Li(FuA)]_x[(P_{4444})(FuA)]_{1-x}$ electrolytes.

two prominent changes are detected upon the addition of Li salt, such as the shift in the position of the resonance line and the increase in the line broadening, suggesting that the local environment of the Li^+ ion changes with increasing salt concentration. The peak full width at half-maxima (FWHM) are 12.88, 14.87, 18.48, and 17.57 Hz for 2.5, 5, 7.5, and 10 mol % Li electrolytes, respectively. The same phenomenon was previously reported for LiFSI in the $[C_3mpyr][FSI]$ IL system.[67] Interestingly, the line width of 7.5 mol % Li electrolytes is larger than that of the electrolyte with 10 mol % Li salt, which is also slightly more deshielded (^{7}Li resonance line at 1.17 ppm) compared with the other three electrolytes with a ^{7}Li resonance line at 1.15 ppm. In these electrolytes, the NMR line-width shape and chemical shifts are affected by the quadrupolar interaction because ^{7}Li has a quadrupole moment.[52] A similar phenomenon was recently observed for NaFSI and NaTFSI salts dissolved in ammonium-based IL, as ^{23}Na has an even larger quadrupole moment than ^{7}Li.[68] The higher amount of Li salt in the IL increases the electrostatic interactions between Li^+ and the $(FuA)^-$ anion and, therefore, decreases the Li^+ ion mobility within the electrolytes. This is one of the main causes for the lower ionic conductivity and ion diffusivity with an increase in the Li salt quantity. The ^{31}P NMR spectra of these electrolytes remained unchanged with an increase in Li salt concentration, suggesting no or negligible interactions of the Li^+ ion with the $(P_{4444})^+$ cation (Figures S4–S7).

FTIR spectroscopy was employed to further understand the specific interactions of the Li^+ ion with various functional groups of the electrolytes. The ATR-FTIR spectra of the neat IL and the electrolytes are shown in Figure S11. The IR bands at 2957–2870, 650–570, and at 1100–1083 cm^{-1} can be assigned to the aliphatic C–H, P–C,[69] and C–O stretchings, respectively. The carboxylic acid C═O stretching appears at around 1750 cm^{-1}. However, the attached functional groups can change the exact position of this band. Figure 8 shows that the $(FuA)^-$ anion carbonyl stretching bands in all samples appeared at 1704–1708 cm^{-1} with shoulders at 1662–1666 cm^{-1}. The carbonyl stretching bands in the $(FuA)^-$ anion are shifted to lower values due to the electrons shifting from the carbonyl toward the furan ring. The electron-withdrawing factor of the furan ring is also facilitating the detachment of the lithium ion from the carbonyl group. Further, the C═C stretching vibrational frequencies in the $(FuA)^-$ anion are also shifted to lower values of 1610–1564 cm^{-1} in comparison to the reference stretching vibrational frequencies of cyclic alkenes (1650–1566 cm^{-1}). This is due to the resonance electron-delocalization promoting more single-bond character within the furan ring.

Electrochemistry. The $(P_{4444})(FuA)$ IL is chosen to prepare high-temperature Li-ion electrolytes for battery applications as this IL has the highest thermal and electrochemical stabilities in comparison to the other ILs having similar chemical structures as reported in our previous work.[18] We checked the solubility of the Li(FuA) salt in the $(P_{4444})(FuA)$ IL to prepare Li-ion battery electrolytes, and the concentration reached a maximum value of 0.305 mol kg^{-1}. Yoon et al. dissolved different salts (LiDCA, LiTFSI, LiFSI, etc.) in the C4mpyr TCB IL and found that the maximum solubility was less than 0.3 mol kg^{-1}.[70] There are many reports where the solubility problem is partly solved by introducing commercial solvents including glymes, but then the unique physicochemical properties such as nonflammability, negligible vapor pressure, and wide ESWs of ILs are sacrificed.[71−75]

The electrochemical studies of the electrolytes are carried out using cyclic voltammetry (CV) and linear sweep voltammetry (LSV). Figure S12 shows that the neat IL and the electrolytes are electrochemically stable and present a

https://doi.org/10.1021/acssuschemeng.1c00939
ACS Sustainable Chem. Eng. 2021, 9, 7769−7780

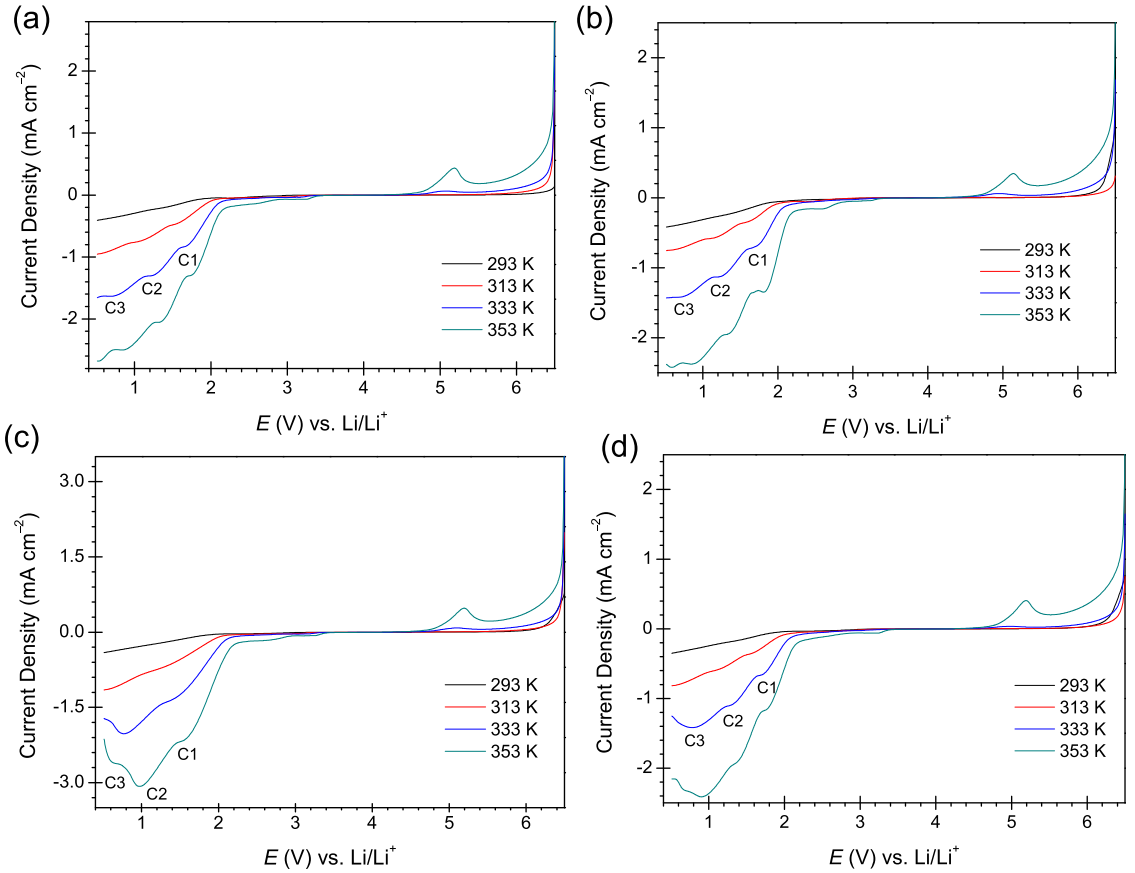

Figure 9. LSV curves of (a) $[Li(FuA)]_{0.025}[(P_{4444})(FuA)]_{0.975}$, (b) $[Li(FuA)]_{0.050}[(P_{4444})(FuA)]_{0.950}$, (c) $[Li(FuA)]_{0.075}[(P_{4444})(FuA)]_{0.925}$, and (d) $[Li(FuA)]_{0.100}[(P_{4444})(FuA)]_{0.900}$ electrolytes on the GC working electrode at different temperatures.

reversible behavior in the potential range from 0.51 to 6.51 V (vs Li/Li$^+$). The electrochemical stability windows (ESWs) of the electrolytes are increasing with an increase in the Li salt concentration. For example, the ESWs of 2.5 mol % Li, 5.0 mol % Li, 7.5 mol % Li, and 10 mol % Li electrolytes are 4.75, 4.83, 4.89, and 4.92 V, respectively, at 293 K. An important characteristic of an electrolyte is its ability to allow electrode reactions efficiently, at the operating temperature of the batteries, without any electrochemical degrading sensations. Therefore, the ESWs of the electrolytes are investigated over a wide temperature range, and the LSV profiles from 293 to 353 K are shown in Figure 9. The ESW data at a 0.1 mA cm^{-2} cutoff current density is given in Table S3. An inverse relationship was observed between temperature and ESWs. With increasing temperature, the ESW of each electrolyte gets narrower, i.e., the $[Li(FuA)]_{0.025}[(P_{4444})(FuA)]_{0.975}$ electrolyte has an ESW of 4.75 V at 293 K, 4.28 V at 313 K, 3.80 V at 333 K, and 2.10 V at 353 K. Thus, the ESW (related to the oxidation and reduction limits) recorded at 353 K differs by 2.65 V with respect to that observed at 293 K.

The decrease in ESWs with temperature might be due to the increase in ionic conductivity and ionic diffusivity, which enables frequent anion/cation contacts with the electrode surface, meaning that the anion oxidation and the cation reduction are temperature dependent.[76] Strongly entrapped water molecules, which are not possible to remove even by high thermal and vacuum treatments, can also decrease the ESWs of IL-based electrolytes.[77,78] A peak at around 5.18 V (vs Li/Li$^+$) in the LSV curves of the electrolytes at 353 K might be due to oxidation of the strongly locked-in water molecules.[78] The current density increases with an increase in the temperature. Above 313 K, three pronounced features C1, C2, and C3 are observed on the cathodic scan side at around 1.66, 1.21, and 0.72 V, respectively (Figure 9). According to the previously published reports,[79] the C1 and C2 peaks can be associated with the underpotential deposition (UPD) of lithium[80,81] and partial decomposition of the $(P_{4444})^+$ cation. The UPD layer formation can modify the nature of the GC working electrode surface, which is beneficial for the extended cathodic limits of the electrolytes where the Li$^+$ ions can pass and prevent further reduction of the $(P_{4444})^+$ cation.[82] The C3 bump in the LSV of the electrolytes at higher temperatures is associated with the reduction of bulk lithium.[79] The Li salt concentration at mid-high temperature exerted a strong influence on the cathodic stability of the electrolytes, thus affecting the electrodeposition of bulk lithium.

The lithium bis(trifluoromethanesulfonyl)imide (LiTFSI) salt solution in imidazolium-, piperidinium-, morpholinium-, and pyrrolidinium-based ILs has been thoroughly investigated for battery applications. The physicochemical, transport, and electrochemical properties of the electrolytes are strongly dependent on the chemical structures of ions, the sizes of ions, the type of electrode surfaces, and the amount of the Li salt added. Generally, stronger ionic interactions between the cation and the anion lead to higher viscosity and lower ion transportation. Kim et al. reported on the mixture of 3-methyl-1-propylimidazolium bis(trifluoromethysulfony)imide (PMIMTFSI) with LiTFSI at a molar ratio of 1:1. The electrolyte showed ionic conductivity up to 0.0012 S cm^{-1}, which is 1 order of magnitude higher than that for a similar

https://doi.org/10.1021/acssuschemeng.1c00939
ACS Sustainable Chem. Eng. 2021, 9, 7769−7780

solution of LiTFSI in the *N*-butyl-*N*-methyl-pyrrolidinium bis(trifluoromethanesulfonyl)imide IL.[83] Further, a similar ionic conductivity value (10^{-3} S cm^{-1}) was obtained when LiTFSI was mixed with the *N*-butyl-*N*-ethylpyrrolidinium bis(trifluoromethanesulfonyl)imide IL.[84] The *N*-ethoxyethyl-*N*-methylpiperidinium FSI and *N*-ethoxyethyl-*N*-methylmorpholinium FSI ILs mixed with LiFSI in a 9:1 molar ratio electrolyte decomposed at 266 °C. These electrolytes presented acceptable ionic conductivity and a suitable electrochemical window with an ability to develop solid electrolyte interfaces on the electrode surfaces.[85] The effect of the anion size on the ionic conductivity of the 1-butyl-3-methylimidazolium cation with six different anions including Cl^-, Br^-, I^-, NCS^-, NCN_2^-, and BF_4^- is also reported.[86] The ionic conductivity increases with increasing anion size, which can be understood from the increase in the anion−cation interaction strength with the ion sizes. In this study, the relatively lower conductivities of the phosphonium furoate-based electrolytes in comparison to those of the reported electrolytes are due to the stronger mutual interactions of ions, which led to slower ion mobility. However, these new electrolytes have shown higher thermal stability and wider electrochemical stability windows. One of the possible approaches to increase the ionic conductivity of these electrolytes is to mix them with conventional organic solvents (acetonitrile)[87] or commercial battery solvents (propylene carbonate),[88] which will effectively hinder the ion association and therefore increase the free mobility of ions. However, this may adversely affect the unique properties of ionic-liquid-based electrolytes.

CONCLUSIONS

The biomass-derived electrolytes comprising the [Li(FuA)] salt and the [(P_{4444})(FuA)] IL exhibited higher thermal stability, acceptable ionic conductivities over a wide temperature range, and wider electrochemical stability windows in the temperature range of 293−353 K. The PFG-NMR analysis revealed that the $(FuA)^-$ anion diffused faster than the $(P_{4444})^+$ cation at all of the concentrations of the added lithium salt. The interactions of the Li^+ ion with the carboxylate group of the anion resulted in slower Li^+ ion diffusion compared with the organic cation and anion. The addition of Li^+ ions decreased the diffusivities of organic ions in a concerted way. Further, the transference number of the Li^+ ion linearly increased with an increase in the Li salt concentration. Three pronounced features were recorded in high-temperature linear sweep voltammetry, presenting lithium underpotential deposition, cation reduction, and lithium bulk reduction. The development of thermally and electrochemically stable fluorine-free, cost-effective, environmentally benign, and sustainable electrolytes will partially meet the challenges associated with the safety, recyclability, accessibility, affordability, and service life of Li-ion batteries. This study will motivate researchers working on batteries and other energy storage devices to look for renewable electrolytes that are produced from biomass on a large scale and move ahead toward sustainable energy storage.

ASSOCIATED CONTENT

Supporting Information

The Supporting Information is available free of charge at https://pubs.acs.org/doi/10.1021/acssuschemeng.1c00939.

Synthesis procedures of lithium salt; NMR and FTIR data; ^1H, ^{13}C, ^7Li, and ^{31}P NMR and FTIR spectra; conductivity VFT equation parameters; Arrhenius plots of the ^1H NMR diffusivity of ions; CV and LSV curves; and anodic limit potentials, cathodic limit potentials, and ESWs (PDF)

AUTHOR INFORMATION

Corresponding Authors

Inayat Ali Khan − *Chemistry of Interfaces, Luleå University of Technology, SE-97187 Luleå, Sweden;* orcid.org/0000-0002-7940-7297; Phone: +46920491738; Email: inayat.khan@ltu.se

Faiz Ullah Shah − *Chemistry of Interfaces, Luleå University of Technology, SE-97187 Luleå, Sweden;* orcid.org/0000-0003-3652-7798; Phone: +46920491291; Email: faiz.ullah@ltu.se

Authors

Oleg Ivanovich Gnezdilov − *Institute of Physics, Kazan Federal University, 420008 Kazan, Russia*

Andrei Filippov − *Chemistry of Interfaces, Luleå University of Technology, SE-97187 Luleå, Sweden; Medical and Biological Physics, Kazan State Medical University, 420012 Kazan, Russia;* orcid.org/0000-0002-6810-1882

Complete contact information is available at: https://pubs.acs.org/10.1021/acssuschemeng.1c00939

Notes

The authors declare no competing financial interest.

ACKNOWLEDGMENTS

The authors would like to thank the Kempe Foundation in memory of J. C. Kempe and Seth M. Kempe for the financial support in the form of a stipend for I.A.K. (grant number SMK-1838). The authors also thank the Swedish Research Council (project number 2018-04133) for financially supporting this work. O.I.G. acknowledges the subsidy allocated to the Kazan Federal University for the state assignment in the sphere of scientific activities (project number 0671-2020-0051).

REFERENCES

(1) Loftus, P. J.; Cohen, A. M.; Long, J. C. S.; Jenkins, J. D. A Critical Review of Global Decarbonization Scenarios: What Do They Tell Us About Feasibility? *Wiley Interdiscip. Rev. Clim. Change* **2015**, *6*, 93−112.

(2) Scrosati, B.; Garche, J. Lithium Batteries: Status, Prospects and Future. *J. Power Sources* **2010**, *195*, 2419−2430.

(3) Wang, Q.; Ping, P.; Zhao, X.; Chu, G.; Sun, J.; Chen, C. Thermal Runaway Caused Fire and Explosion of Lithium Ion Battery. *J. Power Sources* **2012**, *208*, 210−224.

(4) Sloop, S. E.; Pugh, J. K.; Wang, S.; Kerr, J. B.; Kinoshita, K. Chemical Reactivity of PF_5 and $LiPF_6$ in Ethylene Carbonate/Dimethyl Carbonate Solutions. *Electrochem. Solid State Lett.* **2001**, *4*, A42−A44.

(5) Zhang, X.; Ross, P. N., Jr.; Kostecki, R.; Kong, F.; Sloop, S.; Kerr, J. B.; Striebel, K.; Cairns, E. J.; McLarnon, F. Diagnostic Characterization of High Power Lithium-Ion Batteries for Use in Hybrid Electric Vehicles. *J. Electrochem. Soc.* **2001**, *148*, A463−A470.

(6) Zinigrad, E.; Larush-Asraf, L.; Gnanaraj, J. S.; Sprecher, M.; Aurbach, D. On the Thermal Stability of $LiPF_6$. *Thermochim. Acta* **2005**, *438*, 184−191.

(7) Campion, C. L.; Li, W.; Lucht, B. L. Thermal Decomposition of $LiPF_6$-Based Electrolytes for Lithium-Ion Batteries. *J. Electrochem. Soc.* **2005**, *152*, A2327−A2334.
(8) Lu, Z.; Yang, L.; Guo, Y. Thermal Behavior and Decomposition Kinetics of Six Electrolyte Salts by Thermal Analysis. *J. Power Sources* **2006**, *156*, 555−559.
(9) Yang, H.; Zhuang, G. V.; Ross, P. N., Jr. Thermal Stability of $LiPF_6$ Salt and Li-Ion Battery Electrolytes Containing $LiPF_6$. *J. Power Sources* **2006**, *161*, 573−579.
(10) Contestabile, M.; Panero, S.; Scrosati, B. A Laboratory-Scale Lithium-Ion Battery Recycling Process. *J. Power Sources* **2001**, *92*, 65−69.
(11) Vagedes, D.; Erker, G.; Froehlich, R. Synthesis and Structural Characterization of $[H(OEt_2)_2]^+[(C_3H_3N_2)\{B(C_6F_5)_3\}_2]^-$ − a Brønsted Acid With an Imidazole-Derived 'Non-Coordinating' Anion. *J. Organomet. Chem.* **2002**, *641*, 148−155.
(12) Alloin, F.; Sanchez, J.-Y.; Armand, M. B. Conductivity Measurements of LiTFSI Triblock Copolymers with a Central POE Sequence. *Electrochim. Acta* **1992**, *37*, 1729−1731.
(13) Omaru, A.; Nirasawa, T. Secondary Battery and Electrolyte Used Therefore. European Patent EP13185622002.
(14) Barbarich, T. J.; Driscoll, P. F.; Izquierdo, S.; Zakharov, L. N.; Incarvito, C. D.; Rheingold, A. L. New Family of Lithium Salts for Highly Conductive Nonaqueous Electrolytes. *Inorg. Chem.* **2004**, *43*, 7764−7773.
(15) Armand, M.; Johansson, P.; Bukowska, M.; Szczeciński, P.; Niedzicki, L.; Marcinek, M.; Dranka, M.; Zachara, J.; Żukowska, G.; Marczewski, M.; Schmidt, G.; Wieczorek, W. Review-Development of Hückel Type Anions: From Molecular Modeling to Industrial Commercialization. A Success Story. *J. Electrochem. Soc.* **2020**, *167*, No. 070562.
(16) Appetecchi, G. B.; Montanino, M.; Passerini, S. Ionic Liquid-Based Electrolytes for High-Energy Lithium Batteries. In *Ionic Liquids: Science and Applications*; Visser, A. E.; Bridges, N. J.; Rogers, R. D., Eds.; ACS Symposium Series 1117; Oxford University Press, Inc., American Chemical Society: Washington DC, 2013; pp 67−128.
(17) Bonhôte, P.; Dias, A.-P.; Papageorgiou, N.; Kalyanasundaram, K.; Grätzel, M. Hydrophobic, Highly Conductive Ambient-Temperature Molten Salts. *Inorg. Chem.* **1996**, *35*, 1168−1178.
(18) Khan, I. A.; Gnezdilov, O. I.; Wang, Y.-L.; Filippov, A.; Shah, F. U. Effect of Aromaticity in Anion on the Cation-Anion Interactions and Ionic Mobility in Fluorine-Free Ionic Liquids. *J. Phys. Chem. B* **2020**, *124*, 11962−11973.
(19) Gallezot, P. Process Options for Converting Renewable Feedstocks to Bioproducts. *Green Chem.* **2007**, *9*, 295−302.
(20) Lucas, N.; Kanna, N. R.; Nagpure, A. S.; Kokate, G.; Chilukuri, S. Novel Catalysts for Valorization of Biomass to Value-Added Chemicals and Fuels. *J. Chem. Sci.* **2014**, *126*, 403−413.
(21) Taarning, E.; Nielsen, I. S.; Egeblad, K.; Madsen, R.; Christensen, C. H. Chemicals from Renewables: Aerobic Oxidation of Furfuryl and Hydroxymethylfurfural over Gold Catalysts. *ChemSusChem* **2008**, *1*, 75−78.
(22) Lange, J. P.; van der Heide, E.; van Buijtenen, J.; Price, R. Furfural- A Promising Platform for Lignocellulosic Biofuels. *ChemSusChem* **2012**, *5*, 150−166.
(23) Corma, A.; Iborra, S.; Velty, A. Chemical Routes for the Transformation of Biomass into Chemicals. *Chem. Rev.* **2007**, *107*, 2411−2502.
(24) Khan, I. A.; Shah, F. U. Fluorine-Free Ionic Liquid-Based Electrolyte for Supercapacitors Operating at Elevated Temperatures. *ACS Sustainable Chem. Eng.* **2020**, *8*, 10212−10221.
(25) Tanner, J. E. Use of the stimulated echo in NMR diffusion studies. *J. Chem. Phys.* **1970**, *52*, 2523−2526.
(26) Fredlake, C. P.; Crosthwaite, J. M.; Hert, D. G.; Aki, S. N. V. K.; Brennecke, J. F. Thermophysical Properties of Imidazolium-Based Ionic Liquids. *J. Chem. Eng. Data* **2004**, *49*, 954−964.
(27) Maton, C.; Vos, N. D.; Stevens, C. V. Ionic Liquid Thermal Stabilities: Decomposition Mechanisms and Analysis Tools. *Chem. Soc. Rev.* **2013**, *42*, 5963−5977.
(28) Neale, A. R.; Murphy, S.; Goodrich, P.; Hardacre, C.; Jacquemin, J. Thermophysical and Electrochemical Properties of Ethereal Functionalised Cyclic Alkylammonium-Based Ionic Liquids as Potential Electrolytes for Electrochemical Applications. *ChemPhysChem* **2017**, *18*, 2040−2057.
(29) Xue, Z.; Qin, L.; Jiang, J.; Mu, T.; Gao, G. Thermal, Electrochemical and Radiolytic Stabilities of Ionic Liquids. *Phys. Chem. Chem. Phys.* **2018**, *20*, 8382−8402.
(30) Ishikawa, M.; Sugimoto, T.; Kikuta, M.; Ishiko, E.; Kono, M. Pure Ionic Liquid Electrolytes Compatible with a Graphitized Carbon Negative Electrode in Rechargeable Lithium-Ion Batteries. *J. Power Sources* **2006**, *162*, 658−662.
(31) Han, H.-B.; Zhou, S.-S.; Zhang, D.-J.; Feng, S.-W.; Li, L.-F.; Liu, K.; Feng, W.-F.; Nie, J.; Li, H.; Huang, X.-J. Lithium Bis(fluorosulfonyl)imide (LiFSI) as Conducting Salt for Nonaqueous Liquid Electrolytes for Lithium-ion Batteries: Physicochemical and Electrochemical Properties. *J. Power Sources* **2011**, *196*, 3623−3632.
(32) McEwen, A. B.; Ngo, H. L.; Lecompte, K.; Goldman, J. L. Electrochemical Properties of Imidazolium Salt Electrolytes for Electrochemical Capacitor Applications. *J. Electrochem. Soc.* **1999**, *146*, 1687−1695.
(33) Shah, F. U.; Gnezdilov, O. I.; Khan, I. A.; Filippov, A.; Slad, N. A.; Johansson, P. Structural and Ion Dynamics in Fluorine-Free Oligoether Carboxylate Ionic Liquid-Based Electrolytes. *J. Phys. Chem. B* **2020**, *124*, 9690−9700.
(34) Pope, C. R.; Kar, M.; MacFarlane, D. R.; Armand, M.; Forsyth, M.; O'Dell, L. A. Ion Dynamics in A Mixed-Cation Alkoxy-Ammonium Ionic Liquid Electrolyte for Sodium Device Applications. *ChemPhysChem* **2016**, *17*, 3187−3195.
(35) Strate, A.; Neumann, J.; Overbeck, V.; Bonsa, A.-M.; Michalik, D.; Paschek, D.; Ludwig, R. Rotational and Translational Dynamics and their Relation to Hydrogen Bond Lifetimes in an Ionic Liquid by Means of NMR Relaxation Time Experiments and Molecular Dynamics Simulation. *J. Chem. Phys.* **2018**, *148*, No. 193843.
(36) Noda, A.; Hayamizu, K.; Watanabe, M. Pulsed-Gradient Spin-Echo ^1H and ^{19}F Ionic Diffusion Coefficient, Viscosity, and Ionic Conductivity of Non-Chloroaluminate Room-Temperature Ionic Liquids. *J. Phys. Chem. B* **2001**, *105*, 4603−4610.
(37) Tokuda, H.; Hayamizu, K.; Ishii, K.; Susan, A. B. H.; Watanabe, M. Physicochemical Properties And Structures Of Room Temperature Ionic Liquids. 2. Variation of Alkyl Chain Length in Imidazolium Cation. *J. Phys. Chem. B* **2005**, *109*, 6103−6110.
(38) Tokuda, H.; Hayamizu, K.; Ishii, K.; Susan, A. B. H.; Watanabe, M. Physicochemical Properties and Structures of Room Temperature Ionic Liquids. 1. Variation of Anionic Species. *J. Phys. Chem. B* **2004**, *108*, 16593−16600.
(39) Tokuda, H.; Ishii, K.; Susan, A. B. H.; Tsuzuki, S.; Hayamizu, K.; Watanabe, M. Physicochemical Properties and Structures of Room Temperature Ionic Liquids. 3. Variation of Cationic Structures. *J. Phys. Chem. B* **2006**, *110*, 2833−2839.
(40) Tokuda, H.; Tsuzuki, S.; Susan, A. B. H.; Hayamizu, K.; Watanabe, M. How Ionic are Room-Temperature Ionic Liquids? An Indicator of the Physicochemical Properties. *J. Phys. Chem. B* **2006**, *110*, 19593−19600.
(41) Sangoro, J. R.; Iacob, C.; Naumov, S.; Valiullin, R.; Rexhausen, H.; Hunger, J.; Buchner, R.; Strehmel, V.; Kärger, J.; Kremer, F. Diffusion in Ionic Liquids: The Interplay Between Molecular Structure and Dynamics. *Soft Matter* **2011**, *7*, 1678−1681.
(42) Hayamizu, K.; Tsuzuki, S.; Seki, S.; Umebayashi, Y. Nuclear Magnetic Resonance Studies on the Rotational and Translational Motions of Ionic Liquids Composed of *1*-Ethyl-*3*-Methylimidazolium Cation and Bis(Trifluoromethanesulfonyl)amide and Bis-(Fluorosulfonyl)amide Anions and Their Binary Systems Including Lithium Salts. *J. Chem. Phys.* **2011**, *135*, No. 084505.
(43) Annat, G.; MacFarlane, D. R.; Forsyth, M. Transport Properties in Ionic Liquids and Ionic Liquid Mixtures: The Challenges of NMR Pulsed Field Gradient Diffusion Measurements. *J. Phys. Chem. B* **2007**, *111*, 9018−9024.

https://doi.org/10.1021/acssuschemeng.1c00939
ACS Sustainable Chem. Eng. 2021, 9, 7769−7780

(44) Hayamizu, K.; Tsuzuki, S.; Seki, S. Transport and Electrochemical Properties of Three Quaternary Ammonium Ionic Liquids and Lithium Salt Doping Effects Studied by NMR Spectroscopy. *J. Chem. Eng. Data* **2014**, *59*, 1944−1954.
(45) Filippov, A.; Gnezdilov, O. I.; Hjalmarsson, N.; Antzutkin, O. N.; Glavatskih, S.; Furó, I.; Rutland, M. W. Acceleration of Diffusion in Ethylammonium Nitrate Ionic Liquid Confined Between Parallel Glass Plates. *Phys. Chem. Chem. Phys.* **2017**, *19*, 25853−25858.
(46) Filippov, A.; Shah, F. U.; Taher, M.; Glavatskih, S.; Antzutkin, O. N. NMR Self-Diffusion Study of A Phosphonium Bis(Mandelato)-Borate Ionic Liquid. *Phys. Chem. Chem. Phys.* **2013**, *15*, 9281−9287.
(47) Filippov, A.; Azancheev, N.; Taher, M.; Shah, F. U.; Rabet, P.; Glavatskih, S.; Antzutkin, O. N. Self-diffusion and Interactions in Mixtures of Imidazolium Bis(Nandelato)Borate Ionic Liquids with Poly(Ethylene Glycol): ^{1}H NMR Study. *Magn. Reson. Chem.* **2015**, *53*, 493−497.
(48) Filippov, A.; Azancheev, N.; Shah, F. U.; Glavatskih, S.; Antzutkin, O. N. Self-Diffusion of Phosphonium Bis(Salicilato)Borate Ionic Liquid in Pores of Vycor Porous Glass. *Microporous Mesoporous Mater.* **2016**, *230*, 128−134.
(49) Javed, M. A.; Ahola, S.; Håkansson, P.; Mankinen, O.; Aslam, M. K.; Filippov, A.; Shah, F. U.; Glavatskih, S.; Antzutkin, O. N.; Telkki, V.-V. Structure and Dynamics Elucidation of Ionic Liquids by Multidimensional Laplace NMR. *Chem. Commun.* **2017**, *53*, 11056−11059.
(50) Filippov, A.; Azancheev, N.; Gibaydullin, A.; Bhattacharyya, S.; Antzutkin, O. N.; Shah, F. U. Dynamic Properties of Imidazolium Orthoborate Ionic Liquids Mixed with Polyethylene Glycol Studied by NMR Diffusometry and Impedance Spectroscopy. *Magn. Reson. Chem.* **2018**, *56*, 113−119.
(51) Shah, F. U.; Gnezdilov, O. I.; Filippov, A. Ion Dynamics in Halogen-Free Phosphonium Bis(Salicylato)Borate Ionic Liquid Electrolytes for Lithium-Ion Batteries. *Phys. Chem. Chem. Phys.* **2017**, *19*, 16721−16730.
(52) Shah, F. U.; Gnezdilov, O. I.; Gusain, R.; Filippov, A. Transport and Association of Ions in Lithium Battery Electrolytes Based on Glycol Ether Mixed with Halogen-Free Orthoborate Ionic Liquid. *Sci. Rep.* **2017**, *7*, No. 16340.
(53) Menjoge, A.; Dixon, J.; Brennecke, J. F.; Maginn, E. J.; Vasenkov, S. Influence of Water on Diffusion in Imidazolium-Based Ionic Liquids: A Pulsed Field Gradient NMR Study. *J. Phys. Chem. B* **2009**, *113*, 6353−6359.
(54) Brinkkötter, M.; Mariani, A.; Jeong, S.; Passerini, S.; Schönhoff, M. Ionic Liquids in Li Salt electrolyte: Modifying the Li^+ Transport Mechanism by Coordination to an Asymmetric Anion. *Adv. Energy Sustainability Res.* **2021**, *2*, No. 2000078.
(55) Yuan, K.; Bian, H.; Shen, Y.; Jiang, B.; Li, J.; Zhang, Y.; Chen, H.; Zheng, J. Coordination Number of Li^+ in Nonaqueous Electrolyte Solutions Determined by Molecular Rotational Measurements. *J. Phys. Chem. B* **2014**, *118*, 3689−3695.
(56) Nair, A. S.; Banerjee, P.; Sarkar, S.; Bagchi, B. Dynamics of Linear Molecules in Water: Translation-Rotation Coupling in Jump Motion Driven Diffusion. *J. Chem. Phys.* **2019**, *151*, No. 034301.
(57) Larsson, K. E. Rotational and Translational Diffusion in Complex Liquids. *Phys. Rev.* **1968**, *167*, No. 171.
(58) Hayamizu, K.; Aihara, Y.; Price, W. S. Correlating the NMR Self-Diffusion and Relaxation Measurements with Ionic Conductivity in Polymer Electrolytes Composed of Cross-Linked Poly(ethylene oxide-propylene oxide) Doped with $LiN(SO_2CF_3)_2$. *J. Chem. Phys.* **2000**, *113*, 4785−4793.
(59) Hayamizu, K.; Tsuzuki, S.; Seki, S.; Umebayashi, Y. Multinuclear NMR Studies on Translational and Rotational Motion for Two Ionic Liquids Composed of BF_4 Anion. *J. Phys. Chem. B* **2012**, *116*, 11284−11291.
(60) Vogel, H. D. Das Temperaturabhaengigkeitsgesetz der Viskositaet von Fluessigkeiten. *Phys. Z.* **1921**, *22*, 645−646.
(61) Fulcher, G. S. Analysis of Recent Measurements of the Viscosity of Glasses. *J. Am. Ceram. Soc.* **1925**, *8*, 339−355.
(62) Tammann, G.; Hesse, W. Z. The Dependence of the Viscosity on the Temperature in Supercooled Liquids. *Z. Anorg. Allg. Chem.* **1926**, *156*, 245−257.
(63) Frömling, T.; Kunze, M.; Schönhoff, M.; Sundermeyer, J.; Roling, B. Enhanced Lithium Transference Numbers in Ionic Liquid Electrolytes. *J. Phys. Chem. B* **2008**, *112*, 12985−12990.
(64) Gélinas, B.; Natali, M.; Bibienne, T.; Li, Q. P.; Dollé, M.; Rochefort, D. Electrochemical and Transport Properties of Ions in Mixtures of Electroactive Ionic Liquid and Propylene Carbonate with a Lithium Salt for Lithium-Ion Batteries. *J. Phys. Chem. C* **2016**, *120*, 5315−5325.
(65) Martins, V. L.; Sanchez-Ramirez, N.; Ribeiro, M. C. C.; Torresi, R. M. Two Phosphonium Ionic Liquids with High Li^+ Transport Number. *Phys. Chem. Chem. Phys.* **2015**, *17*, 23041−523051.
(66) Brinkkötter, M.; Giffin, G. A.; Moretti, A.; Jeong, S.; Passerini, S.; Schönhoff, M. Relevance of Ion Clusters for Li Transport at Elevated Salt Concentrations in $[Pyr_{12O1}][FTFSI]$ Ionic Liquid-Based Electrolytes. *Chem. Commun.* **2018**, *54*, 4278−4281.
(67) Yoon, H.; Best, A. S.; Forsyth, M.; MacFarlane, D. R.; Howlett, P. C. Physical Properties of High Li-Ion Content *N*-Propyl-*N*-Methylpyrrolidinium Bis(Fluorosulfonyl)Imide Based Ionic Liquid Electrolytes. *Phys. Chem. Chem. Phys.* **2015**, *17*, 4656−4663.
(68) Hilder, M.; Gras, M.; Pope, C. R.; Kar, M.; MacFarlane, D. R.; Forsyth, M.; O'Dell, L. A. Effect of Mixed Anions on the Physicochemical Properties of a Sodium Containing Alkoxyammonium Ionic Liquid Electrolyte. *Phys. Chem. Chem. Phys.* **2017**, *19*, 17461−17468.
(69) Daasch, L. W.; Smith, D. C. Infrared Spectra of Phosphorous Compounds. *Anal. Chem.* **1951**, *23*, 853−868.
(70) Yoon, H.; Lane, G. H.; Shekibi, Y.; Howlett, P. C.; Forsyth, M.; Best, A. S.; MacFarlane, D. R. Lithium Electrochemistry and Cycling Behaviour of Ionic Liquids Using Cyano Based Anions. *Energy Environ. Sci.* **2013**, *6*, 979−986.
(71) Scheers, J.; Pitawala, J.; Thebault, F.; Kim, J.-K.; Ahn, J.-H.; Matic, A.; Johansson, P.; Jacobsson, P. Ionic Liquids and Oligomer Electrolytes Based on the $B(CN)_4^-$ Anion; Ion Association, Physical and Electrochemical Properties. *Phys. Chem. Chem. Phys.* **2011**, *13*, 14953−14959.
(72) Tamura, T.; Hachida, T.; Yoshida, K.; Tachikawa, N.; Dokko, K.; Watanabe, M. New Glyme−Cyclic Imide Lithium Salt Complexes as Thermally Stable Electrolytes for Lithium Batteries. *J. Power Sources* **2010**, *195*, 6095−6100.
(73) Seki, S.; Takei, K.; Miyashiro, H.; Watanabe, M. Physicochemical and Electrochemical Properties of Glyme-$LiN(SO_2F)_2$ Complex for Safe Lithium-ion Secondary Battery Electrolyte. *J. Electrochem. Soc.* **2011**, *158*, A769−A774.
(74) Yoshida, K.; Tsuchiya, M.; Tachikawa, N.; Dokko, K.; Watanabe, M. Correlation between Battery Performance and Lithium Ion Diffusion in Glyme−Lithium Bis(Trifluoromethanesulfonyl)-amide Equimolar Complexes. *J. Electrochem. Soc.* **2012**, *159*, A1005−A1012.
(75) Ueno, K.; Yoshida, K.; Tsuchiya, M.; Tachikawa, N.; Dokko, K.; Watanabe, M. Glyme−Lithium Salt Equimolar Molten Mixtures: Concentrated Solutions or Solvate Ionic Liquids? *J. Phys. Chem. B* **2012**, *116*, 11323−11331.
(76) Wang, Y.-L.; Golets, M.; Li, B.; Sarman, S.; Laaksonen, A. Interfacial Structures of Trihexyltetradecylphosphonium-bis-(mandelato)borate Ionic Liquid Confined Between Gold Electrodes. *ACS Appl. Mater. Interfaces* **2017**, *9*, 4976−4987.
(77) Schröder, U.; Wadhawan, J. D.; Compton, R. G.; Marken, F.; Suarez, P. A. Z.; Consorti, C. S.; de Souza, R. F.; Dupont, J. Water-Induced Accelerated Ion Diffusion: Voltammetric Studies in 1-Methyl-3-[2,6-(S)-dimethylocten-2-Yl]-imidazolium Tetrafluoroborate, 1-Butyl-3-methyl-imidazolium Tetrafluoroborate and Hexafluorophosphate Ionic Liquids. *New J. Chem.* **2000**, *24*, 1009−1015.
(78) Silvester, D. S.; Compton, R. G. Electrochemistry in Room Temperature Ionic Liquids: A Review and Some Possible Applications. *Z. Phys. Chem.* **2006**, *220*, 1247−1274.

https://doi.org/10.1021/acssuschemeng.1c00939
ACS Sustainable Chem. Eng. 2021, 9, 7769−7780

(79) Dilasari, B.; Jung, Y.; Kim, G.; Kwon, K. Effect of Cation Structure on Electrochemical Behavior of Lithium in [NTf_2]-based Ionic Liquids. *ACS Sustainable Chem. Eng.* **2016**, *4*, 491−496.
(80) Wibowo, R.; Jones, S. E. W.; Compton, R. G. Investigating the Electrode Kinetics of the Li/Li^+ in a Wide Range of Room Temperature Ionic Liquids at 298 K. *J. Chem. Eng. Data* **2010**, *55*, 1374−1376.
(81) Gasparotto, L. H. S.; Borisenko, N.; Bocchi, N.; Zein El Abedin, S.; Endres, F. In Situ STM Investigation of the Lithium Underpotential Deposition on Au(111) in the Air- and Water-Stable Ionic Liquid 1-Butyl-1-Methylpyrrolidinium Bis(Trifluoromethylsulfonyl)-amide. *Phys. Chem. Chem. Phys.* **2009**, *11*, 11140−11145.
(82) Howlett, P. C.; Brack, N.; Hollenkamp, A. F.; Forsyth, M.; MacFarlane, D. R. Characterization of the Lithium Surface in *N*-Methyln-Alkylpyrrolidinium Bis(Trifluoromethanesulfonyl)amide Room-Temperature Ionic Liquid Electrolytes. *J. Electrochem. Soc.* **2006**, *153*, A595−A606.
(83) Kim, J.-K.; Matic, A.; Ahn, J.-H.; Jacobsson, P. An Imidazolium Based Ionic Liquid Electrolyte for Lithium Batteries. *J. Power Sources* **2010**, *195*, 7639−7643.
(84) Fernicola, A.; Croce, F.; Scrosati, B.; Watanabe, T.; Ohno, H. LiTFSI-BEPyTFSI as an Improved Ionic Liquid Electrolyte for Rechargeable Lithium Batteries. *J. Power Sources* **2007**, *174*, 342−348.
(85) Tsurumaki, A.; Ohno, H.; Panero, S.; Navarra, M. A. Novel Bis(Fluorosulfonyl)Imide-Based and Ether-Functionalized Ionic Liquids for Lithium Batteries with Improved Cycling Properties. *Electrochim. Acta* **2019**, *293*, 160−165.
(86) Leys, J.; Rajesh, R. N.; Menon, P. C.; Glorieux, C.; Longuemart, S.; Nockemann, P.; Pellens, M.; Binnemans, K. Influence of the Anion on the Electrical Conductivity and Glass Formation of 1-Butyl-3-Methylimidazolium Ionic Liquids. *J. Chem. Phys.* **2010**, *133*, No. 034503.
(87) Rofika, R. N. S.; Honggowiranto, W.; Jodi, H.; Sudaryanto, S.; Kartini, E.; Hidayat, R. The Effect of Acetonitrile as an Additive on the Ionic Conductivity of Imidazolium-Based Ionic Liquid Electrolyte and Charge-Discharge Capacity of its Li-ion Battery. *Ionics* **2019**, *25*, 3661−3671.
(88) Wang, M.; Shan, Z.; Tian, J.; Yang, K.; Liu, X.; Liu, H.; Zhu, K. Mixtures of Unsaturated Imidazolium Based Ionic Liquid and Organic Carbonate as Electrolyte for Li-Ion Batteries. *Electrochim. Acta* **2013**, *95*, 301−307.

https://doi.org/10.1021/acssuschemeng.1c00939
ACS Sustainable Chem. Eng. 2021, 9, 7769−7780